

<https://doi.org/10.1038/s42005-024-01547-3>

Oscillating photonic Bell state from a semiconductor quantum dot for quantum key distribution

Check for updates

Matteo Pennacchietti¹, Brady Cunard², Shlok Nahar², Mohd Zeeshan³, Sayan Gangopadhyay², Philip J. Poole³, Dan Dalacu^{3,4}, Andreas Fognini⁵, Klaus D. Jöns⁶, Val Zwiller⁷, Thomas Jennewein², Norbert Lütkenhaus² & Michael E. Reimer^{1,2} ✉

An on-demand source of bright entangled photon pairs is desirable for quantum key distribution (QKD) and quantum repeaters. The leading candidate to generate such pairs is based on spontaneous parametric down-conversion (SPDC) in non-linear crystals. However, its pair extraction efficiency is limited to 0.1% when operating at near-unity fidelity due to multiphoton emission at high brightness. Quantum dots in photonic nanostructures can in principle overcome this limit, but the devices with high entanglement fidelity (99%) have low pair extraction efficiency (0.01%). Here, we show a measured peak entanglement fidelity of $97.5\% \pm 0.8\%$ and pair extraction efficiency of 0.65% from an InAsP quantum dot in an InP photonic nanowire waveguide. We show that the generated oscillating two-photon Bell state can establish a secure key for peer-to-peer QKD. Using our time-resolved QKD scheme alleviates the need to remove the quantum dot energy splitting of the intermediate exciton states in the biexciton-exciton cascade.

Developing a bright, deterministic source of entangled photon pairs for applications in photonic quantum information processing¹, quantum communication² and networks³, and enhanced imaging techniques^{4–6} has been a long-standing scientific and technological challenge. One promising candidate is based on III-V semiconductor quantum dots (QDs) in photonic nanostructures^{7–10}. Such QDs have shown deterministic polarization-entangled photon pair emission via the biexciton (XX)-exciton (X) cascade and high pair-extraction efficiencies over 30%^{8–10}. However, since semiconductor QDs are hosted in a solid-state environment, dephasing of the exciton spin was a common concern due to interactions with the surrounding nuclear spins of the atomic lattice and spins of free/trapped charges^{11,12}. Therefore, it was presumed that because of indium's large nuclear spin of 9/2, indium-based QDs were unlikely to match the near-unity degree of entanglement (i.e., concurrence $\geq 95\%$) of GaAs QDs, whose nuclei both have smaller nuclear spins of $3/2$ ^{13,14}.

Another common concern is the QD exciton fine-structure splitting (FSS), which causes the two-photon entangled state to oscillate between two

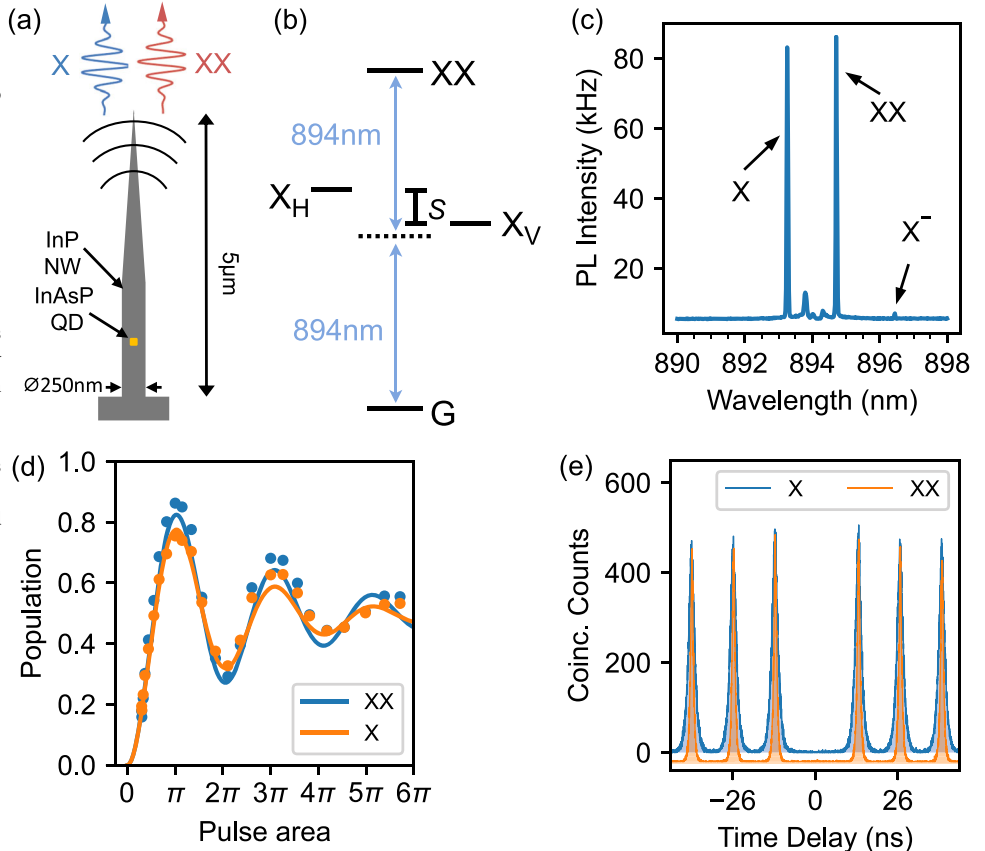
Bell states¹⁵. There have been two main approaches to overcoming the issue of the FSS to maintain high entanglement fidelity: directly removing the FSS using, for example, strain fields¹⁶, or using a low-jitter detection system to time-gate coincidences^{15,17–19}. It was thought that the latter approach was not useful in applications since photon pairs are discarded to select a specific Bell state.

In this article, we show that a time-resolved quantum key distribution (QKD) protocol allows all photon pairs emitted from the biexciton-exciton cascade to generate a secure key, even in the presence of the FSS. To estimate the potential key rates for the protocol, we used the density matrices reconstructed from a 'time-resolved' quantum state tomography experiment (QST) on photon pairs emitted by an InAsP QD in a site-selected tapered InP nanowire waveguide (NW-QD), see Fig. 1a. From the time-resolved QST experiment, we measured the peak concurrence and fidelity of photon pairs to be $95.3 \pm 0.5\%$ and $97.5 \pm 0.8\%$, respectively. This near-unity concurrence was achieved using two-photon resonant excitation (TPRE), see Fig. 1b, and superconducting nanowire single-photon detectors

¹Institute for Quantum Computing and Department of Electrical and Computer Engineering, University of Waterloo, Waterloo, ON N2L 3G1, Canada. ²Institute for Quantum Computing and Department of Physics and Astronomy, University of Waterloo, Waterloo, ON N2L 3G1, Canada. ³National Research Council of Canada, Ottawa, ON K1A 0R6, Canada. ⁴University of Ottawa, Ottawa, ON K1N 6N5, Canada. ⁵Single Quantum B.V., Delft 2628 CJ, The Netherlands. ⁶Institute for Photonic Quantum Systems (PhoQS), Center for Optoelectronics and Photonics Paderborn (CeOPP) and Department of Physics, Paderborn University, Warburger Straße 100, 33098 Paderborn, Germany. ⁷Department of Applied Physics, Royal Institute of Technology, Albanova University Centre, 106 91, Stockholm, Sweden.

✉ e-mail: michael.reimer@uwaterloo.ca

Fig. 1 | Resonant excitation of the nanowire quantum dot. **a** Illustration of the InAsP quantum dot (QD) in an InP tapered nanowire waveguide, which emits the biexciton (XX) and exciton (X) into the same Gaussian mode. **b** Illustration of two-photon resonant excitation (TPRE) generating a biexciton in the QD. The intermediate exciton energy level has a finite fine structure splitting (S) between the H-polarized (X_H) and the V-polarized (X_V) states. **c** The emission spectrum from the nanowire QD under π -pulse TPRE. Exciton and biexciton emission lines are located at 893.25 nm and 894.67 nm, respectively. The small central peaks are from remnants of the filtered laser pulse midway between X and XX. We observe a small contribution from the negatively charged exciton (X^-). **d** Biexciton and exciton state population as a function of pulse area where a pulse area of π corresponds to the maximum population. The dots represent experimental data and the solid curves are the fitted curves (see Supplementary Note 1). **e** Hanbury-Brown-Twiss autocorrelation measurements of both the X and XX emission, demonstrating low multi-photon emission probability.



(SNSPDs) with ultra-low timing jitter (<20 ps) and dark count rate (~1 Hz). The time-resolved nature of the experiment enabled us to measure high values of concurrence over the entire exciton lifetime, resulting in a lifetime-weighted concurrence and fidelity of $90.2 \pm 0.2\%$ and $94.0 \pm 0.1\%$, respectively. Previous measurements of the same NW-QD entangled photon source performed without using TPRE and an optimized detection system yielded much lower values of peak and lifetime-weighted concurrence of $77 \pm 2\%$ and $62 \pm 3\%$, respectively¹⁵. The stark increase in concurrence observed in this study validates the prediction that optimized experimental conditions will increase the measured concurrence on the same QD, and substantiates the initial claim that spin dephasing was not the main factor limiting the measured entanglement fidelity in previous studies of NW-QD entangled photon sources^{7,15,20,21}. We further rigorously prove the security of our proposed time-resolved QKD protocol with more detailed optical models as compared to previous QKD experiments with QDs²²⁻²⁴.

Employing NW-QDs to produce entangled photon pairs with near-unity entanglement fidelity comes with a number of attractive features, including deterministic site-selected growth²⁵, intrinsically low exciton FSS²⁶, potential pair-extraction efficiencies of over 90%^{27,28}, near-unity fabrication yields of bright QDs²⁹, Gaussian emission profile with 93% coupling efficiency of single photons to a single-mode fibre³⁰, and wavelength emission variance from QDs of less than 5 nm³¹. These facts together with the high entanglement fidelity presented in this work illuminate a clear path for the deployment of large arrays of bright, entangled photon pair sources for quantum photonic technologies.

Results

Two photon resonant excitation

Experimental results of TPRE on the NW-QD using laser pulses of ~13 ps (see Methods) are shown in Fig. 1. In Fig. 1c, we observe that the exciton (X) and biexciton (XX) dominate the emission spectrum with the small peaks between X and XX corresponding to remnants of the laser excitation pulse.

We observe three full Rabi cycles in the count rates vs. the pulse area in Fig. 1d, confirming that we are coherently exciting the biexciton state. The oscillations dampen out and settle to the 0.5 population point due to exciton-phonon interactions³².

We fit the count rate vs. pulse area data to determine an estimate for the probability of occupying the XX state after excitation (see Methods). At the π -pulse, we find a XX and X population of 0.82 ± 0.01 and 0.77 ± 0.01 , respectively, (see Supplementary Note 1) resulting in a pair generation efficiency of 0.63 ± 0.01 . Using the measured count rates of 150 kHz for XX and 145 kHz for X under pulsed excitation (76.2 MHz), and the optical setup efficiency of 2.4%, we estimate a pair extraction efficiency at the first lens of $0.65\% \pm 0.02\%$ (see Methods). Luminescence blinking (see Supplementary Note 2) and imperfect generation efficiency are responsible for the reduction in efficiency under TPRE as compared to the efficiency under quasi-resonant excitation (see Supplementary Note 3).

To quantify the multi-photon emission probability under TPRE we perform a Hanbury-Brown-Twiss experiment. The resulting histogram is displayed in Fig. 1e. Ignoring blinking and using only the nearest neighbour peaks around zero time delay we calculate $g_X^{(2)}(0) = 0.0055 \pm 0.0003$ and $g_{XX}^{(2)}(0) = 0.0028 \pm 0.0003$. We observe that $g_{XX}^{(2)}(0)$ is reduced by over an order of magnitude by TPRE as compared to previous work on the same NW-QD using quasi-resonant excitation ($g_{XX}^{(2)}(0) = 0.10 \pm 0.01$)¹⁵.

Influence of detection system

In addition to the excitation technique, there are two main performance metrics of the detector that degrades the measured degree of entanglement. The first is detector dark counts, which is well understood and adds uncorrelated coincidences similar to multi-photon emission. The second is the finite timing resolution of the detection system (i.e., timing jitter), which is largely unexplored and can reduce the measured concurrence when the exciton FSS is non-zero. The FSS is a splitting of the two intermediate

exciton states¹⁶ that causes the exciton spin state to oscillate between $|\uparrow\downarrow\rangle$ (-1 angular momentum) and $|\downarrow\uparrow\rangle$ ($+1$ angular momentum) with a period of $T_S = h/S$, where S is the energy of the FSS. The resulting polarization state of the entangled photon pair emitted via the biexciton-exciton cascade will evolve temporally as:

$$\begin{aligned}
 |\psi(\tau)\rangle &= \frac{1}{\sqrt{2}} [\cos(S\tau/2\hbar)(|RL\rangle + |LR\rangle) \\
 &\quad + i \sin(S\tau/2\hbar)(|RR\rangle + |LL\rangle)] \\
 &= \frac{1}{\sqrt{2}} (|HH\rangle + e^{iS\tau/\hbar}|VV\rangle),
 \end{aligned}
 \tag{1}$$

where $\tau = t_X - t_{XX}$ is the time delay between the emission of the exciton photon and the biexciton photon. The first and second letter denotes the polarization of the biexciton and exciton photon, respectively. The effect of the FSS is a purely local unitary transformation of the exciton spin, implying the state in Eq. (1) is maximally entangled over the entire exciton lifetime¹⁵. However, if the finite timing resolution of the detection system is larger than the FSS oscillation period, then the measured concurrence will be reduced since the phase relationship between $|HH\rangle$ and $|VV\rangle$ in Eq. (1) will be averaged out. This effect can be circumvented by using single-photon detectors with a timing resolution much less than the FSS oscillation period.

Quantum state tomography

We carried out an over-complete quantum state tomography (QST)³³ experiment using TPRES and fast SNSPDs with individual detector timing

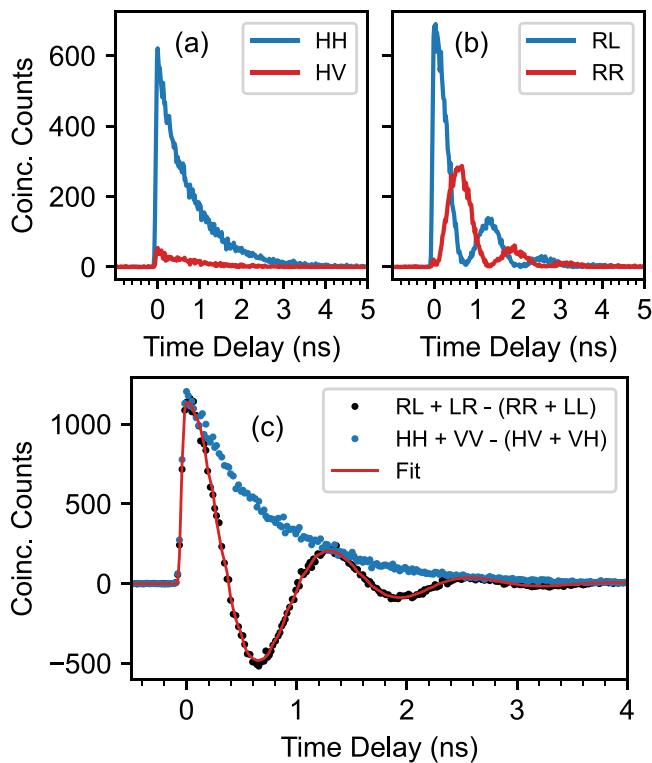


Fig. 2 | Time-resolved quantum state tomography with superconducting nanowire single photon detectors (SNSPDs). **a** Coincidence counts versus time delay (τ) for the HH and HV polarization projection measurements. **b** Coincidence counts versus time delay (τ) for the RL and RR polarization projection measurements. **c** Combinations of coincidence measurements for the states in Eq. (1) versus time delay. The combinations of circular basis measurements $RL + LR - (RR + LL)$ display quantum oscillations between two Bell states. The red curve is the best fit of the oscillations in the circular basis to $\cos(S\tau/\hbar)$ convolved with a Gaussian distribution of fixed FWHM of 30 ps to account for the small amount of blurring from the SNSPD detection system.

jitters of less than 20 ps and very low dark counts rates of $N_d = 1 \pm 1$ Hz. Taking into account both the SNSPDs and the correlation electronics, we estimated a total system timing jitter (full-width-at-half-maximum) of 30 ps (see Methods), which is much faster than the exciton FSS period of the QD under study ($T_S = 1.26$ ns). The QST experiment consisted of a total of 36 separate projective measurements on the joint biexciton-exciton polarization state (see Supplementary Note 4). A subset of the 36 projection measurements captured using the SNSPDs is plotted in Fig. 2a (HH, HV) and Fig. 2b (RL, RR). The coincidence counts from HH follow an exponential decay since the exciton spin state $|\uparrow\downarrow\rangle + |\downarrow\uparrow\rangle$ is a stationary state of the exchange Hamiltonian when the FSS is present³⁴. We see high suppression of coincidences in the HV basis as compared to the HH basis, as expected for a highly entangled state. In contrast, the RL and RR states are not eigenstates of the exchange Hamiltonian when the FSS is present. Thus, the coincidences histogram for the RR and RL basis, displayed in Fig. 2b oscillates $\pi/2$ out of phase with each other.

Equation (1) predicts the oscillation between two Bell states, $(|RL\rangle + |LR\rangle)/\sqrt{2}$ and $(|RR\rangle + |LL\rangle)/\sqrt{2}$, with frequency S/h . We found that plotting the individual measured coincidences in the form of $RL + LR - (RR + LL)$ reveals quantum oscillations between these two Bell states (Fig. 2c). We extract the FSS by fitting the quantum oscillations (red curve in Fig. 2c), yielding 3.226 ± 0.004 μ eV (780.0 ± 1.0 MHz). In contrast, the combination of $HH + VV - (HV + VH)$ follows an exponential decay. By fitting this decay, we extract the radiative exciton lifetime of $\tau_X = 0.777 \pm 0.003$ ns (see Supplementary Note 5).

Concurrence under resonant excitation

With the 36 time-resolved coincidence measurements we reconstruct the density matrix, within a time window of 50 ps as a function τ , using an algorithm based on the maximum likelihood estimation (MLE)³³ method implemented in Python³⁵. From these reconstructed density matrices we calculate the time-resolved concurrence³⁶. In Fig. 3a we plot the concurrence versus time delay for measurements taken using TPRES and SNSPDs with low dark counts and precise timing jitter (green curve). As a

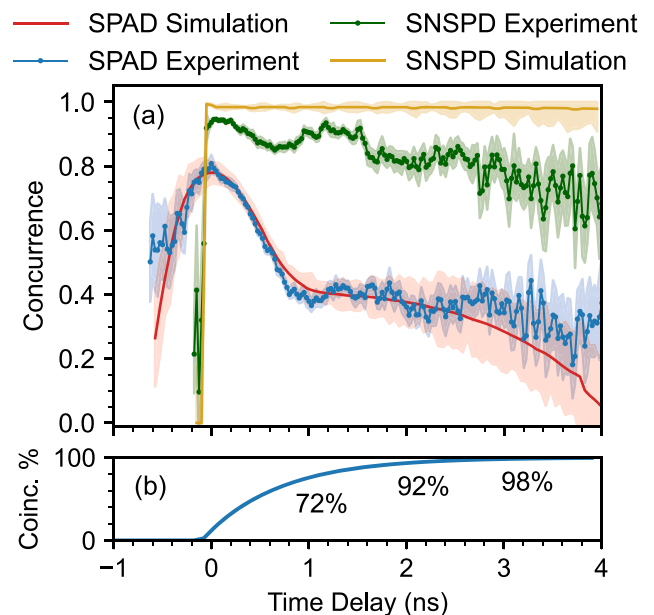


Fig. 3 | Near-unity concurrence from a nanowire quantum dot. **a** Concurrence from reconstructed density matrices as a function of time delay for experimental data and simulated data with time windows of 50 ps. Data is presented for the nanowire quantum dot excited under two-photon resonant excitation at π -pulse using both single photon avalanche diodes (SPADs) and superconducting nanowire single photon detectors (SNSPDs). The shaded regions represent one standard deviation. **b** Percentage of total coincidence counts as a function of time delay.

comparison, we also plot the measured concurrence (blue curve) on the same QD using TPRES and single-photon avalanche diodes (SPADs), which have significantly higher dark count rates and timing jitter (see Methods). The prominent effect of the detection system on the measured concurrence on the same QD is immediately evident from the difference in the two measured curves acquired using SNSPDs versus SPADs.

Due to the large timing jitter of the SPADs (see Supplementary Note 6), XX-X coincidences are recorded when $\tau < 0$. As τ increases and more XX-X coincidences are sampled, there is an initial slow rise of the SPAD concurrence. The increase then slows and reaches a peak of $80 \pm 3\%$ due to phase averaging or blurring of the quantum oscillations, i.e., time-dependent phase information between the two Bell states in Eq. (1). The concurrence then steadily decreases as the detection system samples more of the quantum oscillations, eventually reaching the flat region where the entire detection response function has sampled the temporal evolution of the two-photon entangled state. In stark contrast, there is no distinction between the top and flat regions in the SNSPD concurrence curve. Instead, at $\tau = 0$ the concurrence (fidelity) peaks at $C_p = 95.3 \pm 0.5\%$ ($F_p = 97.5 \pm 0.8\%$), an increase of 24% in the concurrence from the SPAD experiment. We found that taking into account our measured multi-photon emission probability has little effect on the peak concurrence ($95.6 \pm 0.7\%$) and fidelity ($97.7 \pm 0.4\%$). For the time-resolved entanglement fidelity, see Supplementary Note 7. The concurrence then remains relatively flat for $\tau > 0$. As a result, the lifetime weighted concurrence (fidelity) with the SNSPDs was $\bar{C} = 90.2 \pm 0.2\%$ ($\bar{F} = 94.0 \pm 0.1\%$), which is significantly higher than the lifetime weighted concurrence of $50.8 \pm 0.2\%$ acquired with the SPADs.

After $\tau \geq 2$ ns we enter the roll-off region where the concurrence reduces because the signal-to-dark count ratio begins to decrease as dark counts dominate the coincidences. Again, we notice a distinct difference between the SPAD and SNSPD curves, where the former decreases much more than the latter because the dark count rate of the SPADs (tens to hundreds per second) is significantly higher than the dark count rate of the SNSPDs (one per second).

In addition, in Fig. 3a we plot the time-resolved concurrence versus time delay calculated from a dephasing-free model for the SPADs (red) and SNSPDs (yellow). The dephasing-free model accounts for only experimentally measured parameters: the multi-photon emission probability, the measured count rates of X and XX, the detector dark count rate, and the detector system timing response (see Supplementary Note 8). Similar to Neuwirth et al.³⁷, we ignore the presence of blinking when estimating the impact of multi-photon emission on the modelled concurrence. We observe a strong agreement between the model and the experimental concurrence for the SPADs, with the predicted peak concurrence of $78 \pm 3\%$ (80% experimental) and a root mean squared error value between the model and experimental data of 3% when using 95% of the coincidence counts (see

Supplementary Note 9). In contrast, the simulation for the SNSPDs differs from the experimental data in three areas: (1) at $\tau = 0$ ns; (2) $0 < \tau < 2$ ns; and (3) $\tau > 2$ ns.

(1) At $\tau = 0$ ns. The small discrepancy between the experimental peak concurrence and the $99.1 \pm 0.04\%$ concurrence predicted by the model could be due to the combination of leakage excitation laser photons (see Supplementary Note 10), the interaction of the exciton spin with phonons^{38,39} and/or the large energy splitting caused by resonant excitation via the AC Stark Shift⁴⁰. The first mechanism would result in unwanted correlations from the detection of H-polarized laser photons. The latter two mechanisms act on time scales less than the timing resolution of our detection system, thereby resulting in a small reduction in the measured concurrence.

(2) $0 < \tau < 2$ ns. We note that there is a small oscillation in the measured concurrence between $\tau = 0$ and $\tau = 1.3$ ns, which coincides with the FSS period. This drop in concurrence is not from spin-dephasing since it fully recovers around 1.3 ns. Instead, the concurrence dip might be attributed to the QD emission being slightly polarized due to asymmetry in the nanowire shape and/or the waveplates not being perfect quarter and half.

(3) $\tau > 2$ ns. The divergence of the experimental data from the model in the roll-off region can be explained by spin-scattering of the exciton spin before recombination with a characteristic interaction time of ~ 25 ns (see Supplementary Note 11). Such a dephasing time is over an order of magnitude greater than the exciton lifetime, which is in agreement with previous experimental evidence from the neutral exciton in InGaAs QDs^{11,41}. We note that with the SNSPDs we were able to observe spin-dephasing from InAsP QDs in nanowires, which was not possible with SPADs due to their higher timing jitter. In addition, as illustrated in Fig. 3b, more than 90% of the exciton photons are emitted before the concurrence drops.

Time-resolved entanglement-based QKD

Given that we observe high entanglement fidelity over the entire exciton lifetime, we ask: Is it possible to perform a quantum information task using the oscillating quantum state from Eq. (1) without temporal post-selection? Of course, if the quantum information protocol of interest requires one specific Bell state, the oscillation caused by the FSS is an obstacle. However, for QKD a specific Bell state is not required.

Indeed, we can devise a time-resolved QKD protocol where access to a maximally entangled state of the form $(|HH\rangle + \exp(i\tau/\hbar)|VV\rangle)/\sqrt{2}$ is sufficient to generate a secret key. In this case, we would map H polarized light to the bit 0, and V to the bit 1. This key map from quantum to classical data is expectedly agnostic to the phase of the entangled state. As detailed in Supplementary Note 12, in addition to the key map, the procedure to estimate the state shared between Alice and Bob in the QKD protocol is similar to quantum state tomography. Therefore, since a detection system with low-timing jitter compared to the FSS oscillation period allows us to observe a high concurrence through tomographic reconstruction, we prove in Supplementary Note 12 the state at every τ is able to generate a time-resolved key rate. We further show that our time-resolved analysis is valid for any time-dependent states.

As an example, we consider a time-resolved optical implementation of the six-state protocol⁴². We compute the time-resolved key rate for this protocol, i.e., the number of secret bits produced per two-fold coincidence as a function of time delay τ . This is visualized in Fig. 4, where we compare the key rates for the raw data from the NW-QD (blue curve) with the ideal state $|\psi(t)\rangle$ given in Eq. (1) (black curve), and with $|\psi(t)\rangle$ in the dephasing-free regime under optimized experimental conditions (red curve). The latter represents the highest achievable key rate for a perfect QD source under our experimental conditions. From Fig. 4, we see that the time-resolved key rate is positive up to time delays between the biexciton and exciton emission of $5\tau_X$ ns, implying that all photon pairs from the NW-QD are useful for key generation.

The deviation of the simulated and experimental time-resolved key rate from the perfect state ($r(\tau) = 0.99$) shows that the time-resolved key rate is a

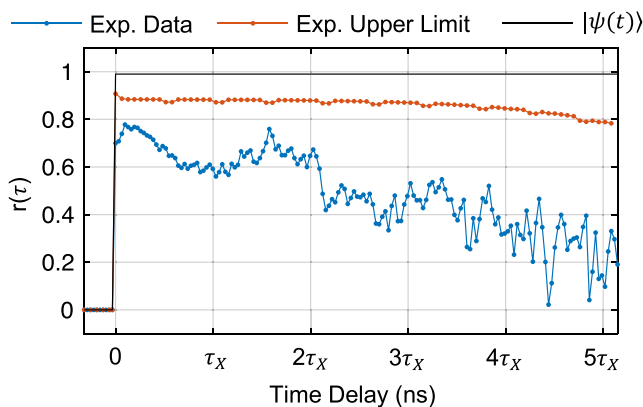


Fig. 4 | Time-resolved key rate. Theoretical key rate for: experimental data (blue) with optimal choice of measurement bases states, dephasing-free model (red) and perfectly oscillating state given by Eq. (1) (black).

more sensitive metric than concurrence since $r(\tau)$ is dependent on the closeness to maximally entangled states in a subspace spanned by Alice and Bob's key map choices. For example, the black curve in Fig. 4 for the perfect state gives the maximum possible key rate as the state oscillates perfectly in the plane spanned by HH and VV . However, the oscillations in the blue curve imply there is no such choice of key map (see Supplementary Notes 7 and 12) for the experimental data. Similarly, the non-zero multi-photon emission probability and finite dark count rate in the simulation, causes the red curve to sit below the perfect state.

We can calculate the number of bits of the secret key produced per excitation pulse R by calculating a lifetime-weighted time-resolved key rate. When averaging from $\tau = 0$ ns to $\tau = 5\tau_X$ we find $R = 0.88$ and $R = 0.64$ for the dephasing-free model and the experimental data, respectively. Note that we have assumed a perfect channel for our proof-of-principle analysis, so the key rate exactly reflects the utility of the source for QKD. In practice, the channel would add some errors and loss which would further degrade this key rate.

Discussion

It is well understood that the exciton FSS will reduce the measured entanglement fidelity defined with respect to one specific Bell state unless temporal post-selection is used^{9,12,14,43}. Thus, if the FSS is not directly removed, then one must settle with either a less efficient entangled photon source or a lower measured entanglement fidelity. In both cases, the overall performance of the entangled photon source is reduced.

Our QKD analysis shows that this trade-off between efficiency and fidelity can be overcome by removing the assumed constraint of requiring only one specific Bell state. Indeed, we constructed a time-resolved QKD protocol where all photon pairs emitted by a QD with non-zero FSS can be used in secret key generation. This protocol works only when the detection system's temporal resolution is much smaller than the FSS period. By implementing our protocol, the key rates in previous QKD experiments with QD entangled photon pair sources^{22–24} could be improved since these experiments did not account for the FSS. In addition, unlike previous security analyses that assume perfect qubit states^{22–24}, we rigorously bound the effect of any multi-photon components of the optical state on the key rate, which is more applicable to practical implementations.

The core experimental challenge with this time-resolved QKD scheme is ensuring that the remote parties are properly synchronized with a temporal resolution much smaller than the FSS oscillation period. If the synchronization timing resolution is of the same order as the FSS oscillation period, then the time-averaged key rate will be reduced, similar to how the time-averaged concurrence is reduced⁴⁴. Thus, a smaller FSS requires a less stringent synchronization resolution to maximize the time-averaged key rate. In the case of small FSS on the order of 5 μ eV, a timing synchronization resolution of less than 50 ps is required. Such accurate timing synchronization is within reach of current technology since it was recently shown that two distant quantum-networked nodes were synchronized to <10 ps over a few kilometres^{45,46}. Thus, it may be less challenging to satisfy the synchronization requirements instead of directly removing the FSS which requires complex fabrication methods^{43,47} or external optics⁴⁴. Therefore, our time-resolved protocol could significantly relax the technical requirements for using bright QD entangled photon sources for peer-to-peer QKD. Fully removing the FSS is likely still needed to realize QD entangled photon sources for building quantum repeaters^{43,48}.

We found that our QD entangled photon source suffers from significant luminescence blinking due to background n-doping of the nanowire (see Supplementary Information of ref. 49). It has been shown in previous work that blinking can be completely removed via the application of an electric field to sweep away excess carriers from the vicinity of the QD⁵⁰. If blinking is successfully removed, our pair extraction efficiency would increase almost six-fold. In addition, techniques to improve the pair generation rate from 80 % to unity can be achieved by optimizing the TPRES pulse⁵¹. Finally, the addition of a gold mirror at the nanowire base should lead to a further two-fold boost of the pair extraction efficiency²⁸.

In summary, we have shown that NW-QD emitters are a bright source of entangled photon pairs with concurrence values that are on par with other leading semiconductor QD devices^{8,10,16,18,19,52}. Our results demonstrated that the low concurrence values found in earlier studies of NW-QD emitters were not due to spin dephasing from the large 9/2 nuclear spin of indium. Instead, imperfect experimental conditions, namely multi-photon emission, detector dark counts, and timing jitter, were the limiting factors. In addition, we found that any residual spin dephasing occurred over time scales that were much longer than the exciton's radiative lifetime. Our findings lay the foundation for creating large arrays of deterministically positioned NW-QDs for QKD networks.

Methods

Quantum dot source

Please refer to ref. 20 for a description of the nanowire quantum dot growth procedure.

Tomography apparatus

A standard cryogenic micro-photoluminescence (PL) apparatus was used to maintain the nanowire sample at 4.5K and enable the optical interfacing via a top window and mirror. Excitation pulses were directed to a 70:30 beamsplitter, with the reflection passing to the micro-PL cryostat. The excitation pulse power was monitored with a photodiode on the transmission port of the 70:30 beamsplitter. After excitation, the photons from exciton and biexciton transition, which are separated by 1 nm in wavelength, couple to the same waveguide mode of the nanowire and then propagate out into free space. The emission from the nanowire is collimated with the objective lens and directed up out of the cryostat. The emission travels through the 70:30 beamsplitter and then three notch filters which filter out the light from the resonant pulse. Then, a transmission grating is used to separate the exciton and biexciton photons into different spatial modes. With the photons separated, we implemented a quantum state tomography setup similar to²¹. Independent polarization transformations were performed on each photon using a $\lambda/4$ followed by a $\lambda/2$ waveplate. Projective polarization measurements were then performed using a polarizer. All four waveplates were mounted inside high-precision, stepper-motorized rotating stages which allowed for automated data-taking and the precise setting of the waveplate principle axes to implement each measurement. The beam was then coupled to a single mode fibre and passed through a fibre-based bandpass filter (full-width-half-max of 0.07 nm) to the single-photon detectors. The electrical signals produced by the detection events are then sent to the two-channel time-tagging electronics. The histogram bin width was set to 16 ps and the integration time for capturing each histogram was 300 s. Please see Supplementary Fig. S11 for an illustration of the experimental apparatus. Please see Supplementary Note 13 for information on how we calibrated the waveplates and determined the measurement settings.

TPRES pulse

For TPRES, a 3 ps pulse from a Mira 900P Ti:Sapphire laser was extended to an approximately 13 ps pulse using a standard 4-f pulse shaper with two 1200 grooves/mm gratings. We note that the temporal duration was not measured directly, instead, we are assuming that the pulse is Fourier-limited, a reasonable assumption to make in the absence of any mechanism introducing chirp into the setup. We have measured a spectral linewidth (full-width-half-max) of 0.08 nm at 894 nm, thus by assuming a Gaussian pulse envelope, the time-bandwidth product gives $\Delta t \approx 0.441/\Delta\nu$.

Detection system

For the detection system, the two SNSPDs (Single Quantum Eos) had a timing resolution of 19 ps and 18 ps, respectively, with the correlation electronics (PicoQuant PicoHarp 300) having a timing resolution of 10 ps. Each exhibits a Gaussian distribution resulting in an overall timing resolution of $\sqrt{19^2 + 18^2 + 2 * 10^2} \approx 30$ ps. The overall detection system timing resolution when using the SPADs was 488 ± 1 ps, see Supplementary

Note 6 for the calculation of this value. The two SPADs had dark count rates of 34 ± 18 and 306 ± 51 , respectively.

Source efficiency

To calculate the efficiency under TPRES, we sent the emission of the nanowire sample directly to a high-resolution diffraction spectrometer. A single SPAD detector was placed at the output of a controllable output split inside the spectrometer to control the selected wavelength of the detector. The efficiency of the collection objective and top mirror of the cryostat is 80% and 95%, respectively. The transmission of the beamsplitter used for mixing in the excitation pulse is 65%. The total optical efficiency after the 70:30 beamsplitter (see Supplementary Note 14) to the SPAD detector after the spectrometer was estimated to be $2.41 \pm 0.07\%$. The unpolarized count rates for both the X and XX emission line were sent to the spectrometer, and the slit was set to record the total count rates in each line. We found 150k counts/sec for the biexciton and 145k counts/s with the exciton. This corresponds to a pair extraction efficiency at the first lens of $0.65 \pm 0.02\%$.

Lifetime-averaged metrics

To calculate the lifetime average we use the equation,

$$\tilde{C} = \frac{\sum_{\tau_n} N_{\tau_n} C(\rho(\tau_n))}{\sum_{\tau_n} N_{\tau_n}} \quad (2)$$

where τ_n is the time bin of the coincidence histogram, $C(\rho(\tau_n))$ is the concurrence of the density matrix ρ reconstructed at time bin τ_n and $N_{\tau_n} = \sum_{ij} N_{\tau_n}^{ij}$ is the sum of all coincidences in the 36 polarization measurements $i, j \in \{H, V, D, A, R, L\}$. Equivalently, we use a similar formula to calculate the key rate

$$R = \frac{\sum_{\tau_n} N_{\tau_n} r(\tau_n)}{\sum_{\tau_n} N_{\tau_n}} \quad (3)$$

where $r(\tau_n)$ is the time-resolved key rate calculated for time delay τ_n . The theoretical basis for this is expanded on in Supplementary Note 12.

Data availability

The experimental data used in this study are available upon request to the corresponding author.

Code availability

The computer code used to reconstruct the density matrices from the experimental data is available on GitHub via ref. 35. Other data analysis scripts used in this study are available upon request from the corresponding author.

Received: 21 August 2023; Accepted: 4 February 2024;

Published online: 24 February 2024

References

- Walther, P. et al. Experimental one-way quantum computing. *Nature* **434**, 169–176 (2005).
- Ekert, A. K. Quantum cryptography based on Bell's theorem. *Phys. Rev. Lett.* **67**, 661–663 (1991).
- Rota, M. B., Basset, F. B., Tedeschi, D. & Trotta, R. Entanglement teleportation with photons from quantum dots: toward a Solid-State based quantum network. *IEEE J. Sel. Top. Quantum Electron.* **26**, 1–16 (2020).
- Nagata, T., Okamoto, R., O'Brien, J. L., Sasaki, K. & Takeuchi, S. Beating the standard quantum limit with four-entangled photons. *Science* **316**, 726–729 (2007).
- Müller, M. et al. Quantum-dot single-photon sources for entanglement enhanced interferometry. *Phys. Rev. Lett.* **118**, 257402 (2017).
- Lemos, G. B. et al. Quantum imaging with undetected photons. *Nature* **512**, 409–412 (2014).
- Jöns, K. D. et al. Bright nanoscale source of deterministic entangled photon pairs violating bell's inequality. *Sci. Rep.* **7**, 1700 (2017).
- Liu, J. et al. A solid-state source of strongly entangled photon pairs with high brightness and indistinguishability. *Nat. Nanotechnol.* **14**, 586–593 (2019).
- Chen, Y., Zopf, M., Keil, R., Ding, F. & Schmidt, O. G. Highly-efficient extraction of entangled photons from quantum dots using a broadband optical antenna. *Nat. Commun.* **9**, 2994 (2018).
- Wang, H. et al. On-Demand semiconductor source of entangled photons which simultaneously has high fidelity, efficiency, and indistinguishability. *Phys. Rev. Lett.* **122**, 113602 (2019).
- Kuhlmann, A. V. et al. Charge noise and spin noise in a semiconductor quantum device. *Nat. Phys.* **9**, 570–575 (2013).
- Kuroda, T. et al. Symmetric quantum dots as efficient sources of highly entangled photons: violation of bell's inequality without spectral and temporal filtering. *Phys. Rev. B Condens. Matter* **88**, 041306 (2013).
- Huber, D. et al. Highly indistinguishable and strongly entangled photons from symmetric GaAs quantum dots. *Nat. Commun.* **8**, 15506 (2017).
- Keil, R. et al. Solid-state ensemble of highly entangled photon sources at rubidium atomic transitions. *Nat. Commun.* **8**, 15501 (2017).
- Fognini, A. et al. Dephasing free photon entanglement with a quantum dot. *ACS Photonics* **6**, 1656–1663 (2019).
- Huber, D. et al. Strain-tunable GaAs quantum dot: a nearly dephasing-free source of entangled photon pairs on demand. *Phys. Rev. Lett.* **121**, 033902 (2018).
- Winik, R. et al. On-demand source of maximally entangled photon pairs using the biexciton-exciton radiative cascade. *Phys. Rev. B Condens. Matter* **95**, 235435 (2017).
- Hopfmann, C. et al. Maximally entangled and gigahertz-clocked on-demand photon pair source. *Phys. Rev. B Condens. Matter* **103**, 075413 (2021).
- Zeuner, K. D. et al. On-Demand generation of entangled photon pairs in the telecom C-Band with InAs quantum dots. *ACS Photonics* **8**, 2337–2344 (2021).
- Versteegh, M. A. M. et al. Observation of strongly entangled photon pairs from a nanowire quantum dot. *Nat. Commun.* **5**, 5298 (2014).
- Huber, T. et al. Polarization entangled photons from quantum dots embedded in nanowires. *Nano Lett.* **14**, 7107–7114 (2014).
- Schimpf, C. et al. Quantum cryptography with highly entangled photons from semiconductor quantum dots. *Sci. Adv.* **7**, eabe8905 (2021).
- Basso Basset, F. et al. Quantum key distribution with entangled photons generated on demand by a quantum dot. *Sci. Adv.* **7**, eabe6379 (2021).
- Dzurnak, B. et al. Quantum key distribution with an entangled light emitting diode. *Appl. Phys. Lett.* **107**, 261101 (2015).
- Dalacu, D. et al. Ultraclean emission from InAsP quantum dots in defect-free wurtzite InP nanowires. *Nano Lett.* **12**, 5919–5923 (2012).
- Singh, R. & Bester, G. Nanowire quantum dots as an ideal source of entangled photon pairs. *Phys. Rev. Lett.* **103**, 063601 (2009).
- Claudon, J., Gregersen, N., Lalanne, P. & Gérard, J.-M. Harnessing light with photonic nanowires: fundamentals and applications to quantum optics. *Chemphyschem* **14**, 2393–2402 (2013).
- Reimer, M. E. et al. Bright single-photon sources in bottom-up tailored nanowires. *Nat. Commun.* **3**, 737 (2012).
- Laferrière, P. et al. Unity yield of deterministically positioned quantum dot single photon sources. *Sci. Rep.* **12**, 6376 (2022).
- Bulgarini, G. et al. Nanowire waveguides launching single photons in a gaussian mode for ideal fiber coupling. *Nano Lett.* **14**, 4102–4106 (2014).

31. Chen, Y. et al. Controlling the exciton energy of a nanowire quantum dot by strain fields. *Appl. Phys. Lett.* **108**, 182103 (2016).
32. Lüker, S. & Reiter, D. E. A review on optical excitation of semiconductor quantum dots under the influence of phonons. *Semicond. Sci. Technol.* **34**, 063002 (2019).
33. James, D. F. V., Kwiat, P. G., Munro, W. J. & White, A. G. Measurement of qubits. *Phys. Rev. A* **64**, 052312 (2001).
34. Bayer, M. et al. Fine structure of neutral and charged excitons in self-assembled In(Ga)As/(Al)GaAs quantum dots. *Phys. Rev. B Condens. Matter* **65**, 195315 (2002).
35. Fokkens, T., Fognini, A. & Zwiller, V. Optical quantum tomography code. <https://github.com/afognini/Tomography/>.
36. Wootters, W. K. Entanglement of formation and concurrence. *Quantum Inf. Comput.* **1**, 27–44 (2001).
37. Neuwirth, J. et al. Multipair-free source of entangled photons in the solid state. *Phys. Rev. B Condens. Matter* **106**, L241402 (2022).
38. Hohenester, U., Pfanner, G. & Seliger, M. Phonon-assisted decoherence in the production of polarization-entangled photons in a single semiconductor quantum dot. *Phys. Rev. Lett.* **99**, 047402 (2007).
39. Cygorek, M. et al. Comparison of different concurrences characterizing photon pairs generated in the biexciton cascade in quantum dots coupled to microcavities. *Phys. Rev. B Condens. Matter* **98**, 045303 (2018).
40. Seidelmann, T. et al. Two-Photon excitation sets limit to entangled photon pair generation from quantum emitters. *Phys. Rev. Lett.* **129**, 193604 (2022).
41. Séné, M., Liu, B. L., Marie, X., Amand, T. & Gérard, J. M. Spin dynamics of neutral and charged excitons in InAs/GaAs quantum dots. In *Optical Properties of 2D Systems with Interacting Electrons* (Springer Netherlands, 2003) 79–88, https://doi.org/10.1007/978-94-010-0078-9_6.
42. Bruß, D. Optimal eavesdropping in quantum cryptography with six states. *Phys. Rev. Lett.* **81**, 3018 (1998).
43. Huber, D., Reindl, M., Aberl, J., Rastelli, A. & Trotta, R. Semiconductor quantum dots as an ideal source of polarization-entangled photon pairs on-demand: a review. *J. Opt.* **20**, 073002 (2018).
44. Fognini, A., Ahmadi, A., Daley, S. J., Reimer, M. E. & Zwiller, V. Universal fine-structure eraser for quantum dots. *Opt. Express* **26**, 24487–24496 (2018).
45. Gerrits, T. et al. White Rabbit-assisted quantum network node synchronization with quantum channel coexistence. In *Conference on Lasers and Electro-Optics, FM1C.2* (Optica Publishing Group, San Jose, California, 2022). https://opg.optica.org/abstract.cfm?URI=CLEO_QELS-2022-FM1C.2.
46. Burenkov, I. A. et al. Synchronization and coexistence in quantum networks. *Opt. Express* **31**, 11431–11446 (2023).
47. Zeeshan, M., Sherlekar, N., Ahmadi, A., Williams, R. L. & Reimer, M. E. Proposed scheme to generate bright entangled photon pairs by application of a quadrupole field to a single quantum dot. *Phys. Rev. Lett.* **122**, 227401 (2019).
48. Yang, J. et al. Statistical limits for entanglement swapping with semiconductor entangled photon sources. *Phys. Rev. B Condens. Matter* **105**, 235305 (2022).
49. Reimer, M. E. et al. Overcoming power broadening of the quantum dot emission in a pure wurtzite nanowire. *Phys. Rev. B Condens. Matter* **93**, 195316 (2016).
50. Zhai, L. et al. Low-noise GaAs quantum dots for quantum photonics. *Nat. Commun.* **11**, 4745 (2020).
51. Kaldewey, T. et al. Coherent and robust high-fidelity generation of a biexciton in a quantum dot by rapid adiabatic passage. *Phys. Rev. B Condens. Matter* **95**, 161302 (2017).
52. Huwer, J. et al. Quantum-dot-based telecommunication-wavelength quantum relay. *Phys. Rev. Appl.* **8**, 024007 (2017).

Acknowledgements

This research was undertaken thanks in part to funding from the Canada First Research Excellence Fund, NSERC (programs Canadian Graduate Scholarship - Masters and Discovery), CMC Microsystems and the Mitacs Accelerate program. We acknowledge the generosity of Single Quantum B.V. for providing us with the superconducting nanowire single-photon detection system for this work.

Author contributions

M.P. performed the experiments with significant contributions from B.C. and M.Z. Data analysis and modelling were performed by M.P. with code developed by A.F. The development and fabrication of the quantum dot emitter was done by D.D. and P.J.P. The superconducting nanowire detectors were provided by A.F. and V.Z. The time-resolved QKD protocol was conceptualized by T.J. and was formalized mathematically by S.N. under the supervision of N.L. with assistance from S.G. Two-photon resonant excitation of the quantum dot was implemented by K.D.J. and M.P. The project was supervised by M.E.R. The paper was written by M.P., S.N. and M.E.R. with input from all authors.

Competing interests

A.F. is employed by Single Quantum and may profit financially. V.Z. is the co-founder and chief scientific officer of Single Quantum and may profit financially. The other authors declare no competing interests.

Additional information

Supplementary information The online version contains supplementary material available at <https://doi.org/10.1038/s42005-024-01547-3>.

Correspondence and requests for materials should be addressed to Michael E. Reimer.

Peer review information *Communications Physics* thanks the anonymous reviewers for their contribution to the peer review of this work. A peer review file is available.

Reprints and permissions information is available at <http://www.nature.com/reprints>

Publisher's note Springer Nature remains neutral with regard to jurisdictional claims in published maps and institutional affiliations.

Open Access This article is licensed under a Creative Commons Attribution 4.0 International License, which permits use, sharing, adaptation, distribution and reproduction in any medium or format, as long as you give appropriate credit to the original author(s) and the source, provide a link to the Creative Commons licence, and indicate if changes were made. The images or other third party material in this article are included in the article's Creative Commons licence, unless indicated otherwise in a credit line to the material. If material is not included in the article's Creative Commons licence and your intended use is not permitted by statutory regulation or exceeds the permitted use, you will need to obtain permission directly from the copyright holder. To view a copy of this licence, visit <http://creativecommons.org/licenses/by/4.0/>.

© The Author(s) 2024